Generalization of the polar representation in time domain fluorescence lifetime imaging microscopy for biological applications: practical implementation

A. LERAY*, C. SPRIET*, D. TRINEL*, Y. USSON†,
& L. HÉLIOT*

Institut de Recherche Interdisciplinaire, USR 3078 CNRS, Université de Lille-Nord de France, BCF, Parc de la Haute Borne, 59650 Villeneuve d'Ascq (France)

†*Laboratoire TIMC-IMAG, UMR 5525 CNRS, Université Joseph Fourier, DyCTiM, Domaine de la Merci, 38710 La Tronche (France)*

Summary

The polar representation or phasor, which provides a fast and visual indication on the number of exponentials present in the intensity decay of the fluorescence lifetime images is increasingly used in time domain fluorescence lifetime imaging microscopy experiments. The calculations of the polar coordinates in time domain fluorescence lifetime imaging microscopy experiments involve several experimental parameters (e.g. instrumental response function, background, angular frequency, number of temporal channels) whose role has not been exhaustively investigated. Here, we study theoretically, computationally and experimentally the influence of each parameter on the polar calculations and suggest parameter optimization for minimizing errors. We identify several sources of mistakes that may occur in the calculations of the polar coordinates and propose adapted corrections to compensate for them. For instance, we demonstrate that the numerical integration method employed for integrals calculations may induce errors when the number of temporal channels is low. We report theoretical generalized expressions to compensate for these deviations and conserve the semicircle integrity, facilitating the comparison between fluorescence lifetime imaging microscopy images acquired with distinct channels number. These theoretical generalized expressions were finally corroborated with both Monte Carlo simulations and experiments.

Correspondence to: Dr. Aymeric Leray, Interdisciplinary Research Institute, CNRS USR 3078, Parc de la Haute Borne, 50 Avenue Halley, 59650 Villeneuve d'Ascq, France. Tel: +33 (0)3 62 53 17 38; fax: +33 (0)3 62 53 17 01; e-mail: aymeric.leray@iri.univ-lille1.fr

Introduction

The fluorescence lifetime defined as the average time that a molecule spends in the excited state before emitting a photon, is an intrinsic fluorophore property sensitive to its local microenvironment. The measurement of the fluorescence lifetimes gives thus access to the surroundings of the fluorescent molecule at the nanometre scale. In conjunction with optical microscopy, fluorescence lifetime imaging microscopy (FLIM) allows to image events such as changes in temperature, pH, ion (e.g. calcium) concentrations and energy transfer occurring in living cells (Lakowicsz, 1999). Currently, FLIM is mainly applied for quantifying protein interaction by measuring Förster resonance energy transfer occurring between two fluorescent probes (a donor and an acceptor) separated by less than 10 nm.

Acceding to the fluorescence lifetime necessitates dedicated systems that are nowadays present in numerous laboratories. These systems are generally subdivided into two main groups; those based on the frequency domain (Gadella *et al.*, 1993; Booth & Wilson, 2004; Leray *et al.*, 2009a) and on the time domain (TD) methods (Cole *et al.*, 2001; Becker *et al.*, 2004; Waharte *et al.*, 2006). The physical principles underlying both methods are identical (translating from TD to frequency domain domain is a simple Fourier transform) but the excitation and detection schemes are totally different. In this work, we focus exclusively on the second group.

In TD FLIM, the fluorescent samples are repeatedly excited by short pulses of light and the resulting fluorescence intensity decay histograms are recorded for each pixel. From these experimental decays, the lifetime components are usually deduced by adjusting each histogram with an exponential

model (Maus *et al.*, 2001; Becker *et al.*, 2004; Waharte *et al.*, 2006). Numerous fitting strategies whose principle consists in minimizing an error function (between the experimental data and the exponential model) with algorithms have been developed and have been used successfully for estimating the lifetime components (Verveer *et al.*, 2000; Barber *et al.*, 2010; Laurence & Chromy, 2010; Trinel *et al.*, 2011). However, this mode of analysis is computation time consuming and requires expertise for obtaining reliable results.

To simplify the analysis and to make it accessible to the nonexpert user, novel methods based on nonfitting approaches have been developed recently (Digman *et al.*, 2008; Padilla-Parra *et al.*, 2008; Leray *et al.*, 2009b). Among them, the polar representation or phasor is increasingly employed in biophysics laboratories (Celli *et al.*, 2010; Stringari *et al.*, 2011). It was initially described for analysing data collected in the frequency domain (Jameson *et al.*, 1984) and has been exhaustively studied by different groups (Clayton *et al.*, 2004; Redford & Clegg, 2005). In brief, it consists in converting the lifetime image into a new two-dimensional histogram called polar or phasor. In this polar representation, each point defined by its [*u*; *v*] coordinates (which are equal to the cosine and sine transforms of the fluorescence intensity decay) corresponds to one pixel of the TD FLIM image and *vice versa*. Consequently, one FLIM image is transformed into a scatter diagram whose position gives an indication on the number of exponentials present in the intensity decay. This approach provides then a fast and visual representation of the fluorescence lifetimes.

This strategy was also recently applied in TD FLIM (Digman *et al.*, 2008; Leray *et al.*, 2009b; Fereidouni *et al.*, 2011). Unlike in frequency domain FLIM where the phase and modulation values (and thus the [*u*; *v*] coordinates) are directly measured by the acquisition system, the polar coordinates in TD FLIM have to be estimated by calculating the Fourier sine and cosine transforms of each temporal histogram. The performance of this approach (in terms of signal-to-noise ratio and minimal number of photons) for TD FLIM experiments has already been studied (Leray *et al.*, 2011). However, we identify several other experimental issues specific to the TD method (e.g. angular frequency of the temporal measurement window, instrumental response function (IRF), background and numerical integrations) that could influence the calculations of the polar coordinates and thus falsify the lifetime estimations. To the best of our knowledge, none of these issues have been exhaustively investigated in the literature.

In this manuscript, we study theoretically, computationally (based on Monte Carlo simulations) and experimentally the influence of each of these issues on the polar calculations and identify possible sources of errors in lifetime calculations. When a bias is introduced in the lifetime estimations, we propose adapted corrections to compensate for it. We finally demonstrate both computationally and experimentally that these corrections, which are applicable with all experimental TD FLIM systems allow retrieving the correct lifetime vales.

Materials and methods

Polar representation

The theory of the standard polar approach for TD FLIM experiments has been detailed previously (Digman *et al.*, 2008; Leray *et al.*, 2011). In brief, the response of a fluorescent sample exhibiting multiple lifetime components to a series of short laser excitation pulses is simply described by a sum of *n* exponentials. However, experimentally, this response is dependent on the IRF of the acquisition system, the finite width *T* of the temporal measurement window and the constant background noted *b* underlying the intensity decays. In this case, the temporal variation of the fluorescence intensity *f(t)* is defined by the convolution product

$$f(t) = \left[\frac{b}{T} + (1-b) \frac{\sum_{i=1}^{n} a_i \exp\left(-\frac{t}{\tau_i}\right)}{\sum_{i=1}^{n} a_i \tau_i \left(1 - \exp\left(-\frac{T}{\tau_i}\right)\right)} \right] \otimes \text{IRF},$$
$$0 \leq t \leq T, \quad (1)$$

which is normalized so that its integral value over *T* equals unity.

The *u*- and *v*-coordinates which correspond to the x- and y-axis of the polar representation are defined by

$$u(\omega) = \frac{\int_0^T f(t) \times \cos(\omega t)\, dt}{\int_0^T f(t)\, dt}, \quad (2)$$

$$v(\omega) = \frac{\int_0^T f(t) \times \sin(\omega t)\, dt}{\int_0^T f(t)\, dt}, \quad (3)$$

where ω is the laser repetition angular frequency. The knowledge of these coordinates gives an indication on the number of exponentials present in the intensity decay. For instance, when the fluorescence emitted by the sample decays mono-exponentially, the coordinates are equivalent to those of a semicircle centred at [0.5; 0] with a radius of 0.5 (see Fig. 1A). Short fluorescence lifetimes are close to the coordinates [1; 0], whereas long lifetimes approach the origin ([0; 0]). If multiple lifetime components are present in the sample, the [*u*; *v*] values no longer correspond to the coordinates of the previously described semicircle (*cf.* Fig. 1A).

The phase and modulation lifetimes τ_m and τ_φ which are well-known parameters in the frequency domain (Lakowicsz, 1999) are related to the [*u*; *v*] coordinates by

$$\tau_\varphi = \frac{1}{\omega}\left(\frac{v}{u}\right) = \frac{1}{\omega}\left(\frac{\int_0^T f(t)\sin(\omega t)\, dt}{\int_0^T f(t)\cos(\omega t)\, dt}\right) \quad (4)$$
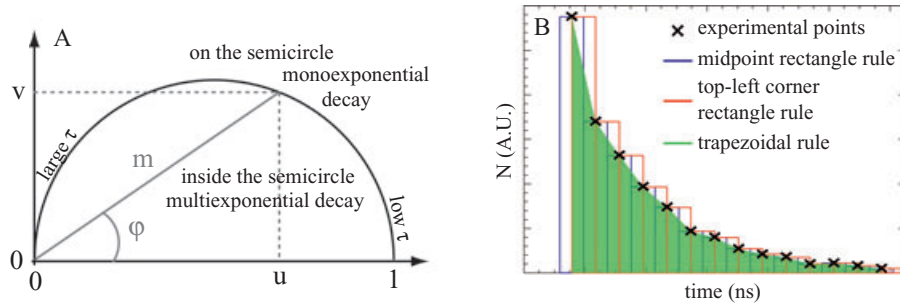
Fig. 1. (A) Illustration of the polar representation. In TD FLIM, the [*u*; *v*] coordinates which correspond to a unique value of phase φ and modulation *m* are calculated by integrating the experimental temporal decays. (B) Different numerical integrations methods can be used. We have represented here the midpoint rectangle rule, the top left corner rectangle rule and the trapezoidal rule.

$$\tau_m = \frac{1}{\omega}\sqrt{\frac{1}{u^2+v^2}-1}$$

$$= \frac{1}{\omega}\sqrt{\frac{\left(\int_0^T f(t)\,dt\right)^2}{\left(\int_0^T f(t)\cos(\omega t)\,dt\right)^2+\left(\int_0^T f(t)\sin(\omega t)\,dt\right)^2}-1}. \tag{5}$$

To help the users to calculate correctly both lifetime values from these expressions, it is crucial to know precisely the influence of each experimental parameter (angular frequency ω, background *b*, IRF . . .). In the next sections of this manuscript, we detail the importance of each parameter based on simulated and experimental data (we limit our study to mono-exponential intensity decays).

Monte Carlo simulations

To evaluate the role of each parameter on the lifetime estimations, we have performed Monte Carlo simulations on a standard computer for generating FLIM images with controlled parameters (more details on the Monte Carlo algorithm can be found in (Spriet *et al.*, 2008; Trinel *et al.*, 2011). To mimic as closely as possible usual experimental conditions, we consider a laser repetition frequency of 80 MHz and a total measurement window width of 12.5 ns which is divided into N_{ch} temporal channels. Each simulated FLIM image was constituted by 64×64 pixels and each pixel corresponds to an intensity histogram composed of a mean of 900 photons. According to the study performed, we can also add a mean number N_b of photons (which are temporally uniformly distributed) to each histogram for modifying the offset *b* or we can vary the full width half maximum (FWHM) of the simulated Gaussian IRF.

Experimental set-up

The TD FLIM images were acquired with the time-correlated single photon counting technique. Our time-correlated single photon counting FLIM system is based on a commercial confocal microscope (Leica TCS SP5 X; Leica Microsystems,

Wetzlar, Germany) coupled with a supercontinuum laser source selected at 485 nm (with an acousto optic tunable filter) with a pulse repetition rate of 80 MHz. Imaging a 1 μM fluorescein solution in pH = 8 Tris buffer was performed with a $63\times$ water immersion objective (NA = 1.2, Leica Microsystems). The resulting fluorescence on the descanned path was selected with a 525/25 bandpass filter and detected with two distinct detectors: a photomultiplier tube (PMT) model PMC100; Hamamatsu, Hamamatsu City, Japan) with a FWHM of 400 ps and a multichannel plate (MCP)-PMT (model R3809U-52; Hamamatsu) with an FWHM of 40 ps Eq. (11). The fluorescence intensity decay histograms were recorded with a dedicated electronic card (SPC 830; Becker & Hickl, Berlin, Germany). The total measurement window which was limited to 10 ns because of severe excitation after-pulses was divided into 64 or 4 temporal channels.

Results and discussion

Importance of the angular frequency ω

The phase and modulation lifetimes defined by Eqs (4) and (5) are directly related to the angular frequency ω [called laser repetition angular frequency by Digman *et al.* (Digman *et al.*, 2008)]. The expressions (4) and (5) are valid if and only if the angular frequency is inversely proportional to the width of the measurement window: $\omega = 2\pi/T$ (first harmonic). In TD FLIM experiments, the first temporal channels are generally dedicated to the evaluation of the experimental background offset. Consequently, the angular frequency ω used in TD FLIM experiments is slightly higher than the laser repetition angular frequency because it corresponds to the angular frequency of the useful measurement window. In that case, we emphasize on the fact that the lifetime's expressions (4) and (5) are not valid and thus the calculated phase and modulation lifetimes are erroneous. To illustrate this phenomenon, we have simulated three FLIM images composed of 64×64 mono-exponential decays with three distinct fluorescence lifetimes (1.0, 2.5 and 4.0 ns) corresponding to standard values usually

Table 1. Influence of the angular frequency ω on the lifetime estimations. The mean phase and modulation lifetimes (τ_m and τ_φ) calculated with three distinct frequencies ($\omega = 2\pi/T_{\text{tot}}$, $\omega = 2\pi/T_{\text{exp}}$ and $\omega = 2\pi/T_{\text{ext}}$) are reported (see text for details) for three simulated lifetime values (1.0, 2.5 and 4.0 ns). The corresponding standard deviations of each quantity are indicated. For the Monte Carlo simulations, we have considered the following parameters: $N = 900$ photons, $N_{\text{ch}} = 64$ channels and $T_{\text{tot}} = 12.5$ ns. We have also reported the theoretical standard deviations calculated from Eqs (9) and (10).

Lifetimes	1.0 (ns)				2.5 (ns)				4.0 (ns)			
	simu	th	simu	th	simu	th	simu	th	simu	th	simu	th
	τ_m	$\Delta\tau_m$	τ_φ	$\Delta\tau_\varphi$	τ_m	$\Delta\tau_m$	τ_φ	$\Delta\tau_\varphi$	τ_m	$\Delta\tau_m$	τ_φ	$\Delta\tau_\varphi$
Total range ($\omega = 2\pi/T_{\text{tot}}$)	0.87 ± 0.04	0.04	0.88 ± 0.03	0.04	2.17 ± 0.10	0.11	2.24 ± 0.15	0.16	3.41 ± 0.20	0.23	4.04 ± 0.55	0.49
Adapted range ($\omega = 2\pi/T_{\text{exp}}$)	1.00 ± 0.04	0.04	1.00 ± 0.04	0.04	2.50 ± 0.12	0.12	2.52 ± 0.20	0.19	4.00 ± 0.26	0.25	4.09 ± 0.66	0.59
Extended range ($\omega = 2\pi/T_{\text{ext}}$)	1.00 ± 0.04	0.04	1.00 ± 0.04	0.04	2.50 ± 0.12	0.11	2.52 ± 0.18	0.17	4.00 ± 0.25	0.24	4.09 ± 0.61	0.54

encountered in FLIM experiments. We have considered a total temporal window of 12.5 ns (corresponding to a laser repetition frequency of 80 MHz) and an initial time $T_{\text{init}} = 1.4$ ns (corresponding to the maximal number of photons). When we calculate the phase and modulation lifetimes with an angular frequency corresponding to the total range ($\omega = 2\pi/T_{\text{tot}}$) different of the experimental range $T_{\text{exp}} = T_{\text{tot}} - T_{\text{init}} = 11.1$ ns, we found wrong lifetime values as indicated in Table 1. By adapting the angular frequency to the experimental measurement window T_{exp} with $\omega = 2\pi/T_{\text{exp}}$, we retrieve the correct phase and modulation lifetime values (Table 1).

We have also investigated the precision of these lifetime measurements for a fluorescent sample whose mono-exponential intensity decay is recorded by an idealized background-free lifetime acquisition system. In this case, the fluorescence emission probability density function $f(t)$ given by Eq. (1) can be simplified as

$$f(t) = \frac{\exp(-t/\tau)}{\tau\left(1 - \exp\left(\frac{-T}{\tau}\right)\right)}, \tag{6}$$

and the [u; v] coordinates are then simply given by

$$u(\omega) = \frac{\int_0^T f(t) \times \cos(\omega t)\, dt}{\int_0^T f(t)\, dt} = \frac{1}{1 + \omega^2\tau^2} \tag{7}$$

$$v(\omega) = \frac{\int_0^T f(t) \times \sin(\omega t)\, dt}{\int_0^T f(t)\, dt} = \frac{\omega\tau}{1 + \omega^2\tau^2}. \tag{8}$$

For this ideal mono-exponential intensity decay, Philip & Carlsson have demonstrated that the precision of the phase lifetime is given by (Philip & Carlsson, 2003)

$$\frac{\Delta\tau_\varphi}{\tau_\varphi} = (1 + \omega^2\tau^2) \times \sqrt{\frac{1 + 2\omega^2\tau^2}{N(1 + 4\omega^2\tau^2)}}. \tag{9}$$

Based on their work, we have also calculated the precision of the modulation lifetime for a mono-exponential intensity

decay. A straightforward calculation leads to

$$\frac{\Delta\tau_m}{\tau_m} = (1 + \omega^2\tau^2) \times \sqrt{\frac{2}{N(1 + 4\omega^2\tau^2)}}. \tag{10}$$

From Eqs (9) and (10), we first remark as expected that the precision of the phase and modulation lifetime is improved when the number of photons N is increased. From these expressions, we also deduce that the precision of the phase and modulation lifetimes is improved when the angular frequency ω decreases and consequently when the measurement window T increases. Of course this measurement window cannot exceed the laser repetition period. One possibility for improving the phase and modulation lifetime precision consists in reducing the number of temporal channels for estimating the background (corresponding to the first temporal channels) and consequently increasing the useful measurement window. In TD FLIM experiment, this implies that the experimental offset has to be evaluated independently (for example by measuring the offset in a nonfluorescent area of the FLIM image). In this case, it becomes possible to slightly extend the useful measurement window T_{ext} from 11.1 to 11.7 ns and consequently to slightly increase the precision of the phase and modulation lifetime values for $\tau = 4$ ns (see Table 1). Note finally that there is a good agreement between the results extracted from the simulations and those calculated from Eqs (9) and (10) (*cf.* Table 1). In the next sections of this manuscript, we consider that the angular frequency is adapted to the experimental measurement window.

Importance of the numerical integration

As previously explained, the polar representation is entirely based on the calculation of the [u; v] coordinates which are theoretically defined as the temporal finite integrals of the product between the fluorescence intensity decay and the sine and cosine functions [*cf.* Eqs (2) and (3)]. In practice, the integral calculations are numerically approximated because
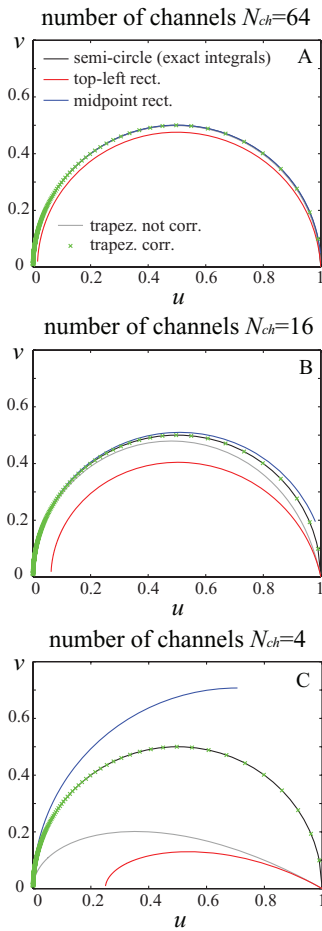
number of channels N_{ch}=64

number of channels N_{ch}=16

number of channels N_{ch}=4

Fig. 2. Influence of the numerical integration method on the polar representations. The polar coordinates of mono-exponential decays with lifetime τ varying from 0 to 30 ns (and $T_{tot} = 12.5$ ns) are calculated with different numerical integration methods (midpoint rectangle rule, top left corner rectangle rule, corrected and not corrected trapezoidal rule) and they are shown for three distinct numbers of temporal channels: $N_{ch} = 4$ (C), 16 (B) and 64 (A). The semicircle of radius 0.5 and centred at [0.5; 0] is also represented in black.

the intensity decay is constituted with a finite number of experimental points. A wide range of methods is available for approximating finite integrals (Davis & Rabinowitz, 1984). The most largely used methods are based on interpolating functions, which are easy to integrate (polynomial of degree zero or one; Davis & Rabinowitz, 1984). Regardless of the method employed, the correct numerical integration of discrete values is the key point for estimating precisely the u- and v-coordinates and thus the phase and modulation lifetimes. When the number of experimental points is large, the numerical integration performed with all these different methods gives comparable accurate results. For a low number of collected data, this is not true. As detailed in the next sections, the error generated with the numerical integration is dependent on the method applied.

Table 2. Influence of the numerical integration method on the $[u; v]$ coordinates calculations. We have reported the minimal number of temporal channels required for obtaining the corresponding accuracy on the polar coordinates with different numerical integration methods (midpoint rectangle rule, top left corner rectangle rule, corrected and not corrected trapezoidal rule).

Numerical integration		Midpoint rectangle rule	Top left corner rectangle rule	Trapezoidal rule not corrected	Trapezoidal rule corrected
$Error_u$	<5% for N_{ch}	≥ 7	≥ 79	≥ 9	≥ 4
	<10% for N_{ch}	≥ 5	≥ 39	≥ 6	≥ 3
	<20% for N_{ch}	≥ 4	≥ 19	≥ 5	≥ 3
$Error_v$	<5% for N_{ch}	≥ 9	≥ 52	≥ 13	≥ 3
	<10% for N_{ch}	≥ 7	≥ 26	≥ 9	≥ 3
	<20% for N_{ch}	≥ 5	≥ 13	≥ 6	≥ 3

(1) Rectangle rule

The simplest numerical integration method consists in approximating the computation of the integral with a sum of rectangles whose width is the temporal resolution and heights are determined by the experimental photon counts multiplied by the sine or cosine functions. Depending upon the rectangle position as a function of the discrete data, different rectangle approximations are possible. If the discrete data correspond to the midpoint of each rectangle (*cf.* Fig. 1B), this numerical integration method is called the midpoint approximation and it has already been detailed (Fereidouni *et al.*, 2011). With this approximation, the calculated polar coordinates (u and v) of a mono-exponential decay are superior to those obtained with exact integration when the number of temporal channels N_{ch} becomes low (Fereidouni *et al.*, 2011). Consequently for low N_{ch} values, the lifetime measurements of fluorescent samples with single exponential decay are no more localized on the semicircle (*cf.* Fig. 2). We have numerically calculated the errors (noted *error$_u$* and *error$_v$*) between the u and v expressions estimated with the midpoint approximation method and those deduced from the exact integrations given by Eqs (7) and (8). For example, the *error$_u$* and *error$_v$* generated during the measurement (with a total temporal window $T = 12.5$ ns) of a sample whose fluorescence lifetime τ is 2.5 ns are inferior to 10% when the number of temporal channels is respectively superior to five and seven (*cf.* Table 2).

In this work, we have also calculated the polar coordinates [for an ideal mono-exponential intensity decay defined by Eq. (6)] by approximating the computation of the integrals reported in Eqs (2) and (3) with a sum of rectangles whose top left corners correspond to the discrete data (*cf.* Fig. 1B). In this case, the coordinates are given by

$$u = \frac{\sum_{t=0}^{N_{ch}} \exp\left(-\frac{t dt}{\tau}\right) \times \cos\left(\frac{2\pi t}{N_{ch}}\right)}{\sum_{t=0}^{N_{ch}} \exp\left(-\frac{t dt}{\tau}\right)} \qquad (11)$$

$$v = \frac{\sum_{t=0}^{N_{ch}} \exp\left(-\frac{t dt}{\tau}\right) \times \sin\left(\frac{2\pi t}{N_{ch}}\right)}{\sum_{t=0}^{N_{ch}} \exp\left(-\frac{t dt}{\tau}\right)} \qquad (12)$$

where N_{ch} is the number of temporal channels and dt is the temporal width of the channel. From the exponential sum formulas, these expressions can be written as

$$u = \frac{\exp\left(\frac{N_{ch} dt}{2\tau}\right)\left(1 - \exp\left(\frac{dt}{\tau}\right)\right)\left[\cos\left(\frac{2\pi}{N_{ch}}\right)\cosh\left(\frac{N_{ch} dt}{2\tau}\right) - \cosh\left(\frac{(N_{ch}+2) dt}{2\tau}\right)\right]}{\left(1 - \exp\left(\frac{(N_{ch}+1) dt}{\tau}\right)\right)\left[\cos\left(\frac{2\pi}{N_{ch}}\right) - \cosh\left(\frac{dt}{\tau}\right)\right]} \qquad (13)$$

$$v = \frac{\left(1 - \exp\left(\frac{dt}{\tau}\right)\right)\left(1 - \exp\left(\frac{N_{ch} dt}{\tau}\right)\right)\sin\left(\frac{2\pi}{N_{ch}}\right)}{2\left(1 - \exp\left(\frac{(N_{ch}+1) dt}{\tau}\right)\right)\left[\cos\left(\frac{2\pi}{N_{ch}}\right) - \cosh\left(\frac{dt}{\tau}\right)\right]}. \qquad (14)$$

As shown in Figure 2, the $[u; v]$ coordinates obtained with this numerical integration method are largely inferior to those deduced from the exact integrals even if $N_{ch} = 64$. The semicircle of radius 0.5 and centred at $[0.5; 0]$ is therefore never conserved for $N_{ch} < 64$ (*cf.* Fig. 2). As previously mentioned, we can easily calculate the errors (noted $error_u$ and $error_v$) introduced by this method of quadrature, in comparison with the exact integrations [defined by Eqs (7) and (8)]. If we consider the previously described example ($T = 12.5$ ns and $\tau = 2.5$ ns), we found that $error_u$ and $error_v$ are inferior to 10% when the numbers of temporal channels are respectively superior to 39 and 26 (*cf.* Table 2). This example illustrates well that both numerical integration methods based on rectangle rule are not equivalent. Special care is thus required in the choice of the method for minimizing the errors.

Finally, regardless of the rectangle rule employed, we should emphasize on the fact that the fluorescence lifetimes (τ_m and τ_φ) cannot be analytically expressed as a function of the polar coordinates (u and v).

(2) Trapezoidal rule

To reduce this integral computation error, a more sophisticated interpolating function (a polynomial of degree 1) has also been considered here (*cf.* Fig. 1B). In brief, the integrals defined by Eqs (2) and (3) are approximated with a sum of trapezoids whose two edges correspond to the discrete data (experimental photon counts multiplied by the sine and cosine functions). In this case, the polar coordinates for a mono-exponential intensity decay defined by Eq. (6) can be expressed as

$$u = \frac{\frac{1}{2}\left(1 + \exp\left(-\frac{N_{ch} dt}{\tau}\right)\right) + \sum_{t=1}^{N_{ch}-1} \exp\left(-\frac{t dt}{\tau}\right)\cos\left(\frac{2\pi t}{N_{ch}}\right)}{\frac{1}{2}\left(1 + \exp\left(-\frac{N_{ch} dt}{\tau}\right)\right) + \sum_{t=1}^{N_{ch}-1} \exp\left(-\frac{t dt}{\tau}\right)} \qquad (15)$$

$$v = \frac{\sum_{t=1}^{N_{ch}-1} \exp\left(-\frac{t dt}{\tau}\right) \times \sin\left(\frac{2\pi t}{N_{ch}}\right)}{\frac{1}{2}\left(1 + \exp\left(-\frac{N_{ch} dt}{\tau}\right)\right) + \sum_{t=1}^{N_{ch}-1} \exp\left(-\frac{t dt}{\tau}\right)} \qquad (16)$$

which, from the exponential sum formulas, leads to

$$u = \frac{-\dfrac{\left(1 - \exp\left(\frac{-N_{ch} dt}{\tau}\right)\right)\sinh\left(\frac{dt}{\tau}\right)}{2\left(\cos\left(\frac{2\pi}{N_{ch}}\right) - \cosh\left(\frac{dt}{\tau}\right)\right)}}{\exp\left(-\frac{N_{ch} dt}{2\tau}\right)\coth\left(\frac{dt}{2\tau}\right)\sinh\left(\frac{N_{ch} dt}{2\tau}\right)}$$

$$= \frac{1}{1 + \operatorname{csch}\left(\frac{dt}{2\tau}\right)^2 \sin\left(\frac{\pi}{N_{ch}}\right)^2} \qquad (17)$$

$$v = \frac{-\dfrac{\sin\left(\frac{2\pi}{N_{ch}}\right)\sinh\left(\frac{N_{ch} dt}{(2\tau)}\right)}{\cos\left(\frac{2\pi}{N_{ch}}\right) - \cosh\left(\frac{dt}{\tau}\right)}}{\coth\left(\frac{dt}{2\tau}\right)\sinh\left(\frac{N_{ch} dt}{2\tau}\right)} = \frac{\sin\left(\frac{2\pi}{N_{ch}}\right)\tanh\left(\frac{dt}{2\tau}\right)}{\cosh\left(\frac{dt}{\tau}\right) - \cos\left(\frac{2\pi}{N_{ch}}\right)}. \qquad (18)$$

These $[u; v]$ coordinates calculated with the trapezoidal rule are reported in Figure 2 for three distinct numbers of temporal channels. We remark that these polar coordinates become inferior to those deduced from the exact integrals (which implies that the semicircle of radius 0.5 and centred at $[0.5; 0]$ is not preserved) when the number of temporal channels is inferior to 16. We have analytically expressed the errors (noted $error_u$ and $error_v$) between the u and v expressions given by Eqs (17) and (18) and those deduced from the exact integrations [defined by Eqs (7) and (8)]. For the same previous example ($T = 12.5$ ns and $\tau = 2.5$ ns), the errors ($error_u$ and $error_v$) generated with the trapezoidal rule are inferior to 10% when the numbers of temporal channels are respectively superior to six and nine (*cf.* Table 2). These errors are thus largely reduced in comparison with those introduced with the top left corner rectangle rule and they are almost identical to those introduced with the midpoint rectangle rule.

However, we should emphasize on the fact that it becomes possible to analytically express the fluorescence lifetime as a function of the polar coordinates (u and v) from the expressions given by Eqs (17) and (18) which is not feasible from those given by Eqs (13) and (14). The phase and modulation lifetimes (τ_φ and τ_m) obtained with the trapezoidal rule can thus be easily calculated. In brief, we simply calculate the ratio v/u of Eqs (17) and 18 (which should be equal to the phase tangent $\tan\varphi$ with exact integrations) and we express the lifetime as a function of this ratio. A straightforward calculation leads to the phase lifetime expression

$$\tau_\varphi = \frac{dt}{\operatorname{arcsinh}\left(\frac{\sin(2\pi/N_{ch}) \times u}{v}\right)}. \qquad (19)$$
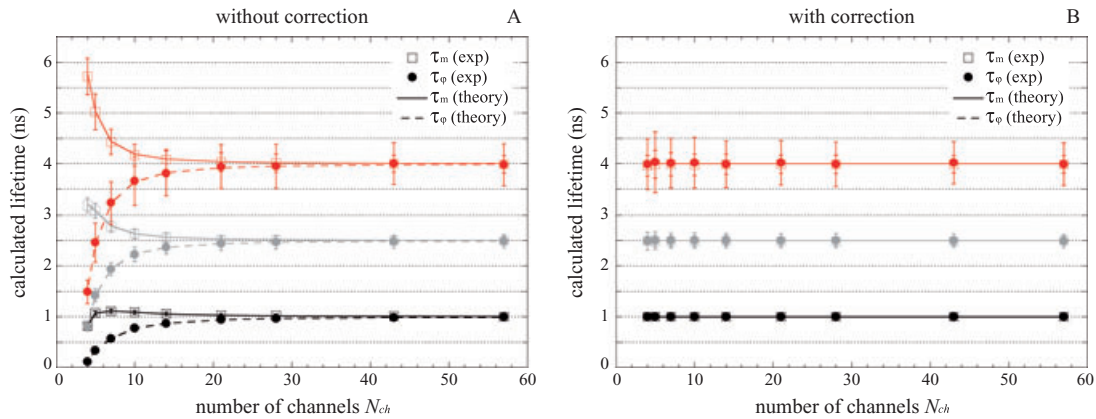
Fig. 3. Comparison of lifetime estimations for mono-exponential decays with and without correction (see text for details). We represented the phase and modulation lifetimes as a function of the number of temporal channels (N_{ch}) with (B) and without (A) correction. Three different fluorescence lifetimes were considered: 1.0 (black), 2.5 (grey) and 4.0 ns (red) with: $N = 900$ photons and $T_{tot} = 12.5$ ns. In both graphs, markers with error bars represent the median fluorescence lifetime calculated with trapezoidal rule and the interquartile ranges of 4096 simulated histograms. The theoretical values which are in excellent agreement with the experimental ones are also indicated with dotted lines.

We also calculate the squared sum of the $[u; v]$ coordinates defined by Eqs (17) and (18) and we resolve the system $u^2 + v^2 = m^2$ for obtaining the modulation lifetime with trapezoidal rule

$$\tau_m = \frac{dt}{2\,\mathrm{arcsech}\left(2\sqrt{\dfrac{(m^2-1)}{m^2-3+(1+m^2)\cos\left(\frac{2\pi}{N_{ch}}\right)-\sqrt{2(m^4-6m^2+1)\cos\left(\frac{2\pi}{N_{ch}}\right)+\frac{\left(1+m^2\right)^2}{2}\left(3+\cos\left(\frac{4\pi}{N_{ch}}\right)\right)}}}\right)}. \tag{20}$$

We finally calculate the corrected polar coordinates with the trapezoidal rule (u and v) by inserting Eqs (19) and (20) into the following expressions

$$u = \left(1 + \omega^2\tau_m^2\right)^{-1/2}\cos(\arctan(\omega\tau_\varphi)) \tag{21}$$

$$v = \left(1 + \omega^2\tau_m^2\right)^{-1/2}\sin(\arctan(\omega\tau_\varphi)). \tag{22}$$

These corrected $[u; v]$ coordinates are indicated in Figure (2) for three distinct numbers of temporal channels. We emphasize on the fact that they are now perfectly superimposable with the semicircle of radius 0.5 and centred at [0.5; 0] even if the number of temporal channels is as low as four. These corrected expressions make it possible to compare directly the data acquired with distinct number of temporal channels N_{ch} because the polar coordinates are no more shifted according to N_{ch}.

To verify that these corrections do not modify the lifetimes, we have computed FLIM images for different number of temporal channels and distinct lifetime values (1.0, 2.5 and 4.0 ns) and we have compared the results obtained with and without correction (*cf.* Fig. 3). We notice that the phase and modulation lifetimes calculated with trapezoidal rule (dots in Fig 3A) are in excellent agreement with those deduced from

Eqs (17) and (18) (indicated with lines in Fig. 3A) and that they diverge from the expected values when the number of temporal channels is reduced (inferior to 20). When the lifetimes are calculated from the corrected expressions [given by Eqs (19) and (20)], the accuracies of both lifetimes are preserved even if the number of temporal channels is as low as four (see Fig. 3B).

Influence of the IRF

The IRF of a FLIM acquisition system is defined as the temporal response of this system to an infinitely short pulse. The IRF is of course extremely dependent on the system. With usual TD FLIM system, its FWHM can vary between 30 ps with a multichannel plate detector (Waharte *et al.*, 2006) and 450 ps with a single photon sensitive avalanche photodiode (Luchowski *et al.*, 2009). The experimental intensity decays, which are equal to the convolution product of the IRF with the theoretical exponential decays are also extremely dependant on the acquisition system. We have then investigated the influence of the size of the IRF on the phase and modulation lifetime calculations. To do this, we consider that the IRF can be approximated with a Gaussian function of mean μ_g and standard deviation σ_g (Grecco *et al.*, 2009). The convolution product of this Gaussian IRF with a single exponential intensity decay recorded by an idealised background-free
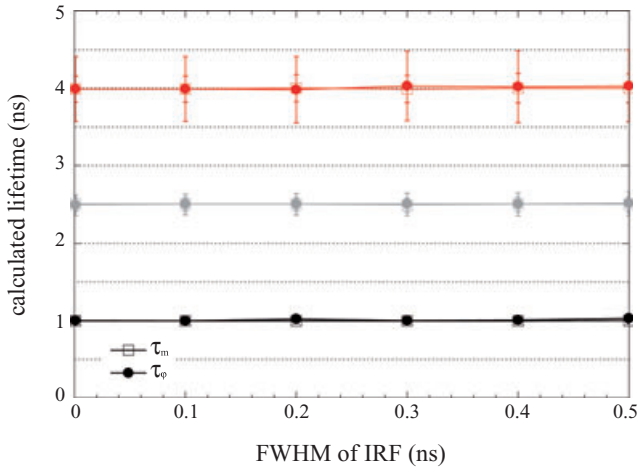
Fig. 4. Role of the temporal width of the instrumental response function (IRF) on the lifetime estimations. The median phase and modulation lifetimes calculated from mono-exponential decays with lifetime $\tau = 1.0$ (black), 2.5 (grey) and 4.0 ns (red) and constituted with $N = 900$ photons dispatched in a temporal window $T_{tot} = 12.5$ ns divided into $N_{ch} = 64$ temporal channels are indicated with markers. The error bars correspond to the interquartile ranges of 4096 simulated histograms.

lifetime acquisition system is given by

$$f(t) = \frac{\exp\left(-\frac{t}{\tau}\right)}{\tau\left(1-\exp\left(-\frac{T}{\tau}\right)\right)} \otimes \frac{\exp\left(-\frac{(t-\mu_g)^2}{2\sigma_g^2}\right)}{\sigma_g\sqrt{2\pi}}$$

$$= \frac{\exp\left(\frac{\sigma_g^2}{2\tau^2}+\frac{\mu_g}{\tau}-\frac{t}{\tau}\right)}{2\tau\left(1-\exp\left(-\frac{T}{\tau}\right)\right)}\left(1-\mathrm{Erf}\left(\frac{\sigma_g}{\tau\sqrt{2}}+\frac{\mu_g-t}{\sigma_g\sqrt{2}}\right)\right), \quad (23)$$

where Erf is the error function. We can thus calculate the polar coordinates (u and v) and the phase and modulation lifetimes (τ_m and τ_φ) by inserting this expression into Eqs (4) and (5). However, there are no simple analytical expressions for τ_m and τ_φ.

We have therefore computed FLIM images with Gaussian IRF of different FWHM for the same fluorescence lifetimes (1.0, 2.5 and 4.0 ns). The corresponding calculated phase and modulation lifetimes reported on Figure 4 indicate that the influence of the IRF temporal width is negligible for mono-exponential intensity decays. The phase lifetimes are indeed identical to the modulation lifetimes and their precisions and accuracies do not depend on the FWHM of the IRF, within the limit of standard deviation.

Importance of the background

In absence of background for a sample with a single exponential intensity decay, the [u; v] coordinates are simply defined by Eqs (7) and (8). By inserting these Eqs (7) and (8) into Eqs (4) and (5) for the fundamental angular frequency ($\omega = 2\pi/T$), a straightforward calculation leads to

$$\tau_\varphi = \tau_m = \tau. \quad (24)$$

In this case, the phase and modulation lifetimes are equal and they correspond to the fluorophore lifetime. If we consider now that there is a constant background noted b underlying the intensity decay, the fluorescence intensity function $f(t)$ is then defined as

$$f(t) = \frac{b}{T} + (1-b)\frac{\exp(-t/\tau)}{\tau\left(1-\exp\left(\frac{-T}{\tau}\right)\right)}, \quad (25)$$

and the [u; v] coordinates become

$$u(\omega) = \frac{\int_0^T f(t)\times\cos(\omega t)\,dt}{\int_0^T f(t)\,dt} = \frac{1-b}{1+\omega^2\tau^2} \quad (26)$$

$$v(\omega) = \frac{\int_0^T f(t)\times\sin(\omega t)\,dt}{\int_0^T f(t)\,dt} = \frac{(1-b)\,\omega\tau}{1+\omega^2\tau^2}. \quad (27)$$

An insertion of Eqs (26) and (27) into Eqs (4) and (5) leads to

$$\tau_\varphi = \tau \quad (28)$$

$$\tau_m = \frac{1}{\omega}\sqrt{\frac{\omega^2\tau^2+2b-b^2}{(1-b)^2}} = \frac{\tau}{1-b}\sqrt{1+\frac{2b-b^2}{\omega^2\tau^2}} \neq \tau. \quad (29)$$

Consequently, the modulation lifetime is not equal to the fluorophore lifetime when background is present. In other words, molecular species with single exponential decay are no more localized on the semicircle centred at [0.5; 0] with a radius of 0.5.

To illustrate this phenomenon, we have computed FLIM images with different background levels. The calculated phase and modulation lifetimes are reported with dots in Figure 5(A). As anticipated from the theory, the phase lifetime corresponds to the simulated value and it is not affected by the background level b. On the contrary, the modulation lifetime is extremely dependent on the background level b and is totally different from the expected lifetime. Figure 5(A) shows also that the results deduced from Monte Carlo simulations are in excellent agreement with those calculated from Eqs (28) and (29) (indicated with lines in Fig. 5A).

For improving the accuracy of the modulation lifetime, it is necessary that the simulated temporal decays are background corrected. To do this, we estimate an average background from a nonfluorescent area that we subtract from the simulated decays. With this process, the phase lifetime is not modified and the modulation lifetime becomes correct (see Fig. 5B). Note also that the background subtraction modifies only the median value of the lifetimes but it does not affect the calculation precision.

Experimental application

To validate the previously described simulated results, we have performed FLIM acquisitions on fluorescein solution with different experimental conditions (IRF, background, number
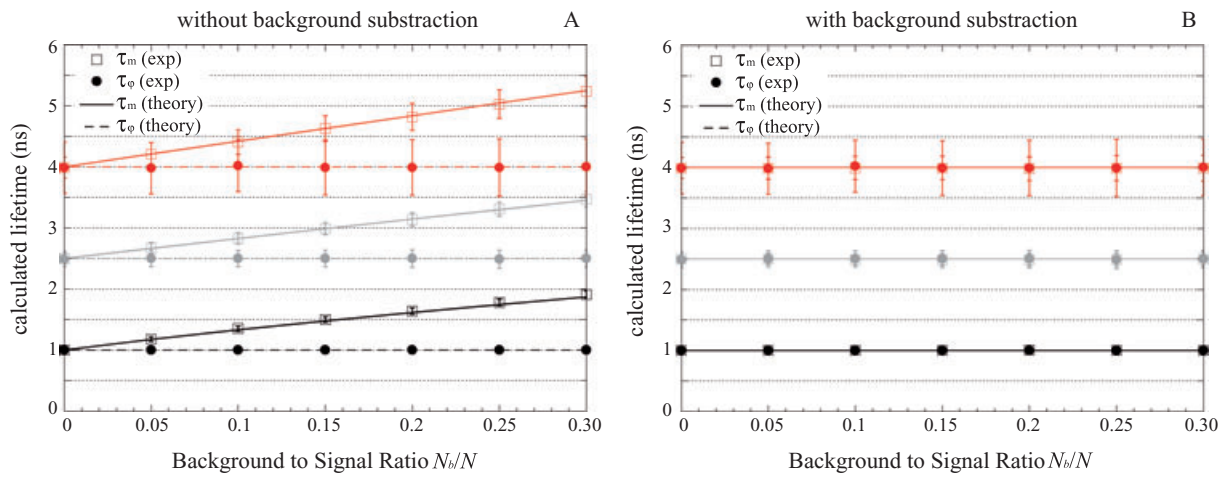
Fig. 5. Plots of the phase and modulation lifetimes for mono-exponential decays as a function of the background to signal ratio (N_b/N). The experimental fluorescence lifetimes (whose median are indicated with markers and error bars correspond to the interquartile ranges of 4096 simulated histograms), which are comparable to the theoretical values (indicated with dotted lines) are reported with (B) and without (A) background subtraction. In both cases, the following parameters were considered: $\tau = 1.0$ (black), 2.5 (grey) and 4.0 ns (red), $N = 900$ photons, $N_{ch} = 64$ temporal channels and $T_{tot} = 12.5$ ns.
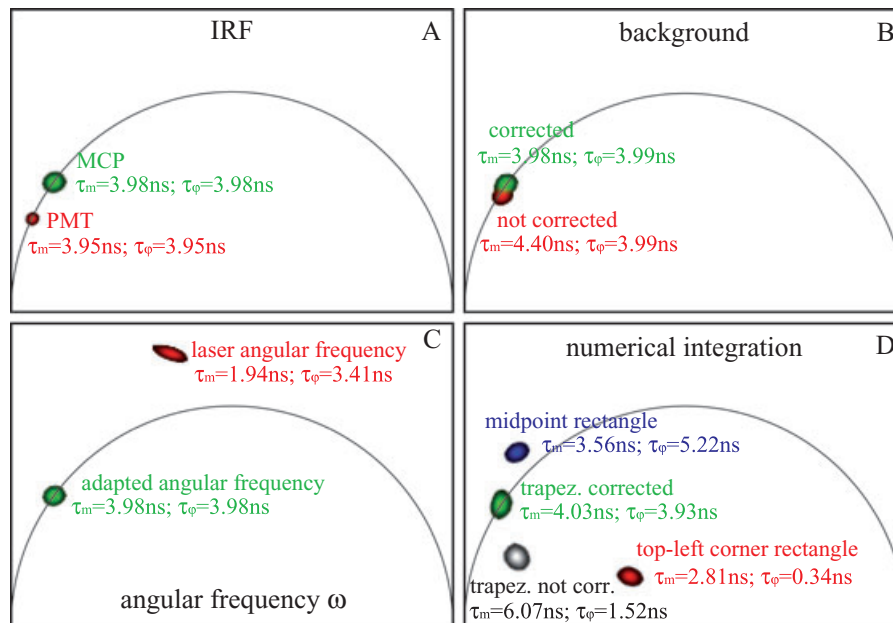
Fig. 6. Experimental illustration of the importance of distinct parameters on the polar representation. (A): Role of the IRF. We have reported the polar representations deduced from FLIM images of a fluorescein solution acquired with two detectors with distinct FWHM: MCP (40 ps) and PMT (400 ps). In both cases, the spot is satisfactorily localized on the semicircle. The resulting phase and modulation lifetimes are also indicated. (B): Influence of the background. We have plotted the polar representation and indicated the corresponding lifetime values, with and without background subtraction (for $N_{ch} = 64$). (C): Role of the angular frequency ω. When the angular frequency is not perfectly adapted to the measurement window, both the polar representation and the lifetimes are erroneous. (D): Importance of the numerical integration method. The polar representations (and the corresponding lifetimes) estimated with all numerical integration methods (midpoint rectangle rule, top left corner rectangle rule and not corrected trapezoidal rule) are aberrant. Only our corrected trapezoidal rule allows retrieving both the correct lifetimes and the expected spot position on the semicircle. In all panels, the number of temporal channels was set to 64 except in (D) where it was fixed to four. If not specified, the detector used for FLIM imaging was the MCP.

of temporal channels). For each condition, we have calculated the [u; v] coordinates and the resulting polar representations are reported on Figure 6.

As expected from our simulations, the temporal width of the IRF (whose FWHM are respectively around 40 ps for the MCP and 400 ps for the PMT) does not modify the phase and modulation lifetimes deduced from TD FLIM images of a fluorescein solution. The two spots calculated with both detectors are well positioned on the semicircle of radius 0.5 and centred at [0.5; 0]. By contrast, the calculated phase and modulation lifetimes values are erroneous if the angular frequency ω is not perfectly adapted to the experimental measurement window (*cf.* Fig 6C) or if the background is not correctly subtracted (*cf.* Fig. 6B). As anticipated, we notice that the presence of the background alters only the modulation lifetime.

The importance of the numerical integration when the fluorescence lifetime is measured with four temporal channels is finally shown in Figure 6D. As already mentioned, for such a low number of temporal channels, all numerical integration methods propagate errors. The previously described corrections are thus indispensable to retrieve both accurate lifetimes and correct spot position on the semicircle (centred at [0.5; 0] with radius 0.5).

Conclusion

We study both theoretically, computationally and experimentally the influence of several experimental parameters on the polar calculations and thus on the phase and modulation lifetime estimations. We demonstrate in this way that the IRF temporal width of the TD FLIM system does not perturb the lifetime calculations, which is not the case for the background underlying the fluorescence decays. However, we show that the errors introduced with this background can be easily compensated with a simple subtraction. To obtain correct lifetime values, we also highlight the fact that the angular frequency ω has to be carefully tuned to the experimental measurement window (and not necessarily to the laser repetition angular frequency).

We finally demonstrate the importance of the choice of the numerical integration method employed for integrals calculations when the number of temporal channels is low ($N_{ch} < 64$). We notably reveal that polar semicircle in not preserved when $N_{ch} = 4$, regardless of the numerical integration method used here (rectangle and trapezoidal rules). To compensate for these deviations from the semicircle, we propose corrected expressions that we validate both with Monte Carlo simulations and FLIM experiments.

In this work, the numerical integrations were performed with simple interpolating functions (polynomial of degree zero and one). Other numerical integration methods exist based on interpolating functions of higher degree [as the Simpson's rule, . . . (Jeffreys & Jeffreys, 1988)] for reducing the integrals computation errors. However, the expressions of the polar coordinates [u; v] are more complicated in this case (not shown). Furthermore, the interest of reducing these computational errors is not obvious insofar as the corrected expressions reported here compensate efficiently these computational errors even if the number of temporal channels is as low as four.

The experimental validation of our corrected expressions was performed here on TD FLIM images acquired with the time-correlated single photon counting technique. However, we emphasize on the fact that our corrected expressions are not restricted to time-correlated single photon counting measurements. They can also be easily applied with TD FLIM images acquired with all existing TD FLIM techniques including those using a streak camera (Krishnan *et al.*, 2003) or a time gated detector (Straub & Hell, 1998; Cole *et al.*, 2001). In this last case, our generalized expressions are particularly adapted because the number of temporal channels is usually low [which implies that the computational errors are substantial if the polar coordinates are not corrected (Fereidouni *et al.*, 2011)].

Finally, tough the study presented here was performed on samples exhibiting mono-exponential intensity decays, our corrected expressions for low channels numbers are general. In other words, our corrected expressions are still applicable for samples emitting multiexponential intensity decays like in Förster resonance energy transfer experiments (see Fig. S1) and they are even indispensable for obtaining correct polar representation when the number of temporal channels is low. Furthermore, the previously described procedures for subtracting the background and for adapting the angular frequency which are also valid whatever the number of lifetime components present in the sample are necessary for true polar localization. All the practical results presented in this manuscript should thus be useful to guide users who are eager to implement the polar representation on their own TD FLIM experiments.

Acknowledgements

References

Barber, P. R., Ameer-Beg, S.M., Pathmananthan, S., Rowley, M. & Coolen, A.C.C. (2010) A Bayesian method for single molecule, fluorescence burst analysis. *Biomed. Opt. Express* **1**, 1148–1158.

Becker, W., Bergmann, A., Hink, M.A., Konig, K., Benndorf, K. & Biskup, C. (2004) Fluorescence lifetime imaging by time-correlated single-photon counting. *Microsc. Res. Tech.* **63**, 58–66.

Booth, M. J. & Wilson, T. (2004) Low-cost, frequency-domain, fluorescence lifetime confocal microscopy. *J. Microsc.* **214**, 36–42.

Celli, A., Sanchez, S., Behne, M., Hazlett, T., Gratton, E. & Mauro, T. (2010) The Epidermal Ca2+ Gradient: measurement Using the Phasor Representation of Fluorescent Lifetime Imaging. *Biophys. J.* **98**, 911–921.

Clayton, A.H., Hanley, Q.S. & Verveer, P.J. (2004) Graphical representation and multicomponent analysis of single-frequency fluorescence lifetime imaging microscopy data. *J. Microsc.* **213**, 1–5.

Cole, M.J., Siegel, J., Webb, S. E. D. *et al.* (2001) Time-domain whole-field fluorescence lifetime imaging with optical sectioning. *J. Microsc.* **203**, 246–257.

Davis, P.J. & Rabinowitz, P. (1984) *Methods of Numerical Integration.* Academic Press, Orlando, Florida.

Digman, M.A., Caiolfa, V.R., Zamai, M. & Gratton, E. (2008) The phasor approach to fluorescence lifetime imaging analysis. *Biophys. J.* **94**, L14–L16.

Fereidouni, F., Esposito, A., Blab, G.A. & Gerritsen, H.C. (2011) A modified phasor approach for analyzing time-gated fluorescence lifetime images. *J. Microsc.* **244**, 248–258.

Gadella, T.W.J., Jovin, T.M. & Clegg, R.M. (1993) Fluorescence lifetime imaging microscopy (flim)—spatial-resolution of microstructures on the nanosecond time-scale. *Biophys. Chem.* **48**, 221–239.

Grecco, H.E., Roda-Navarro, P. & Verveer, P.J. (2009) Global analysis of time correlated single photon counting FRET-FLIMdata. *Opt. Express* **17**, 6493–6508.

Jameson, D.M., Gratton, E. & Hall, R.D. (1984) The measurement and analysis of heterogeneous emissions by multifrequency phase and modulation fluorometry. *Appl. Spectrosc. Rev.* **20**, 55–106.

Jeffreys, H. & Jeffreys, B.S. (1988) *Methods of Mathematical Physics.* Cambridge University Press, Cambridge.

Krishnan, R.V., Saitoh, H., Terada, H., Centonze, V.E. & Herman, B. (2003) Development of a multiphoton fluorescence lifetime imaging microscopy system using a streak camera. *Rev. Sci. Instrum.* **74**, 2714–2721.

Lakowicsz, J.R. (1999) *Principles of Fluorescence Spectroscopy.* Plenum Publishers, New York.

Laurence, T.A. & Chromy, B.A. (2010) Efficient maximum likelihood estimator fitting of histograms. *Nat. Methods* **7**, 338–339.

Leray, A., Riquet, F.B., Richard, E., Spriet, C., Trinel, D. & Heliot, L. (2009a) Optimized protocol of a frequency domain fluorescence lifetime imaging microscope for FRET measurements. *Microsc. Res. Tech.* **72**, 371–379.

Leray, A., Spriet, C., Trinel, D., Blossey, R., Usson, Y. & Héliot, L. (2011) Quantitative comparison of polar approach versus fitting method in time domain FLIM image analysis. *Cytometry Part A* **79A**, 149–158.

Leray, A., Spriet, C., Trinel, D. & Heliot, L. (2009b) Three-dimensional polar representation for multispectral fluorescence lifetime imaging microscopy. *Cytometry A* **75**, 1007–1014.

Luchowski, R., Gryczynski, Z., Sarkar, P., Borejdo, J., Szabelski, M., Kapusta, P. & Gryczynski, I. (2009) Instrument response standard in time-resolved fluorescence. *Rev. Sci. Instrum.* **80**, 033109-1, 033109-6.

Maus, M., Cotlet, M., Hofkens, J., Gensch, T., De Schryver, F C., Schaffer, J. & Seidel, C.A.M. (2001) An experimental comparison of the maximum likelihood estimation and nonlinear least-squares fluorescence lifetime analysis of single molecules. *Anal. Chem.* **73**, 2078–2086.

Padilla-Parra, S., Auduge, N., Coppey-Moisan, M. & Tramier, M. (2008) Quantitative FRET analysis by fast acquisition time domain FLIM at high spatial resolution in living cells. *Biophys. J.* **95**, 2976–2988.

Philip, J. & Carlsson, K. (2003) Theoretical investigation of the signal-to-noise ratio in fluorescence lifetime imaging. *J. Opt. Soc. Am. A* **20**, 368–379.

Redford, G.I. & Clegg, R.M. (2005) Polar plot representation for frequency-domain analysis of fluorescence lifetimes. *J. Fluoresc.* **15**, 805–815.

Spriet, C., Trinel, D., Riquet, F., Vandenbunder, B., Usson, Y. & Heliot, L. (2008) Enhanced FRET contrast in lifetime imaging. *Cytometry A* **73**, 745–753.

Straub, M. & Hell, S.W. (1998) Fluorescence lifetime three-dimensional microscopy with picosecond precision using a multifocal multiphoton microscope. *Appl. Phys. Lett.* **73**, 1769–1771.

Stringari, C., Cinquin, A., Cinquin, O., Digman, M.A., Donovan, P.J. & Gratton, E. (2011) Phasor approach to fluorescence lifetime microscopy distinguishes different metabolic states of germ cells in a live tissue. *Proc. Natl. Acad. Sci. U. S. A.* **108**, 13582–13587.

Trinel, D., Leray, A., Spriet, C., Usson, Y. & Héliot, L. (2011) Upgrading Time Domain FLIM using an adaptive Monte Carlo Data inflation algorithm. *Cytometry Part A* **79A**, 528–537.

Verveer, P.J., Squire, A. & Bastiaens, P.I. (2000) Global analysis of fluorescence lifetime imaging microscopy data. *Biophys. J.* **78**, 2127–2137.

Waharte, F., Spriet, C. & Heliot, L. (2006) Setup and characterization of a multiphoton FLIM instrument for protein-protein interaction measurements in living cells. *Cytometry A* **69**, 299–306.

Supporting Information

Additional supporting information may be found in the online version of this paper:

Fig. S1. Comparison of lifetime estimations for bi-exponential decays with and without correction (set text for details). We plotted the phase and modulation lifetimes as a function of the number of temporal channels (N_{ch}) with (B) and without (A) correction. We considered two simulated FLIM images (with $N = 900$ photons and $T_{tot} = 12.5$ ns); the first one with the following parameters: $\tau_1 = 2.5$ ns, τ_2 4.0 ns, $a_1 = 0.5$ and the second one with: $\tau_1 = 1.0$ ns, $\tau_2 = 2.5$ ns, $a_1 = 0.5$. In both graphs, the median fluorescence lifetime calculated with trapezoidal rule is indicated with markers and the error bars correspond to the interquartile ranges of 4096 simulated histograms. The corrected phase and modulation lifetimes are independent on the number of channels except when they become of the same order as the temporal resolution of the FILM acquisition system.

Please note: Wiley-Blackwell is not responsible for the content or functionality of any supporting materials supplied by the authors. Any queries (other than missing material) should be directed to the corresponding author for the paper.